Blue luminescence of $SrTiO_3$ under intense optical excitation

A. Rubano,[1] D. Paparo,[2] F. Miletto Granozio,[2] U. Scotti di Uccio,[1,2] and L. Marrucci[1,2,a)]
[1]*Dipartimento di Scienze Fisiche, Università di Napoli "Federico II," Complesso Universitario di Monte S. Angelo, v. Cintia, 80126 Napoli, Italy*
[2]*CNR-INFM Coherentia, Complesso Universitario di Monte S. Angelo, v. Cintia, 80126 Napoli, Italy*

(Received 29 July 2009; accepted 30 September 2009; published online 23 November 2009)

The blue-green photoluminescence emitted by pure and electron-doped strontium titanate under intense pulsed near-ultraviolet excitation is studied experimentally as a function of excitation intensity and temperature. Both emission spectra and time-resolved decays of the emission are measured and analyzed in the framework of simple phenomenological models. We find an interesting blue-to-green transition occurring for increasing temperatures in pure samples, which is absent in doped materials. The luminescence yield and decay rate measured as a function of temperature can be modeled well as standard activated behaviors. The leading electron-hole recombination process taking place in the initial decay is established to be second order, or bimolecular, in contrast to recent reports favoring a third-order interpretation as an Auger process. The temporal decay of the luminescence can be described well by a model based on two interacting populations of excitations, respectively identified with interacting defect-trapped (possibly forming excitons) and mobile charges. Finally, from the measured doping and sample dependence of the luminescence yield, we conclude that the radiative centers responsible for the luminescence are probably intrinsic structural defects other than bulk oxygen vacancies. © *2009 American Institute of Physics*. [doi:10.1063/1.3256140]

I. INTRODUCTION

Strontium titanate, or $SrTiO_3$ (STO), is among the most widely investigated perovskite oxides, owing both to its potential for novel electronic applications and to its widespread use as a substrate for the epitaxial growth of strongly correlated electronic materials, such as superconducting cuprates or colossal-magnetoresistive manganites. Recently, the puzzling transport properties of its interface with other insulating oxides have also attracted much interest.[1,2] Despite this large effort, many properties of this material still await a complete clarification.

Intrinsic STO (I-STO) is a band insulator, characterized by a huge static dielectric constant resulting from the rather soft bonding of the small Ti^{4+} ion to the surrounding octahedral O^{2-} cage. Its conduction band (CB) is composed of states having a mainly Ti 3d t_{2g} character, while its valence band (VB) has a dominantly O 2p character, with an upper edge located away from the Γ point in the Brillouin zone.[3] This results in an indirect gap of 3.2–3.3 eV, while the direct (optical) gap is 3.4–3.7 eV, with a non-negligible sample and temperature dependence.[3,4] Upon *n*-type doping, generally achieved either by introducing O vacancies or by chemical substitution (e.g., La^{3+} for Sr^{2+} or Nb^{5+} for Ti^{4+}), STO becomes a conductor with a relatively large low-temperature mobility.[5,6] In this regime, it is known that the charge carriers are dressed by the interaction with the lattice and seem to behave mainly as large polarons, although with several nonstandard features.[6–9] When I-STO is irradiated with ultraviolet (UV) light, photogenerated electrons and holes (e,h) appear to both contribute to the material photoconductivity.[10] Theoretical calculations would also indicate that holes in pure STO are not strongly coupled to phonons and keep their bare mass.[11]

The photoluminescence (PL) properties of STO are possibly even more puzzling and controversial than its transport ones. The greenish luminescence (GL) having a maximum at 2.2–2.4 eV of photon energy (wavelength $\lambda \approx 500$ nm) that is emitted by pure STO at low temperature under exposure to UV or x-ray radiation has been known since a long time[12–14] and is generally ascribed to the decay of intrinsic self-trapped excitons (STEs).[15–18] A STE can be roughly depicted as a tightly bound state of a hole and a Ti^{3+} polaron.[19,20] However, this purely intrinsic scenario has been recently called into question by Mochizuki *et al.*,[21,22] who argued for a crucial role of defects and possibly of surfaces in this GL emission.

Only recently, another PL emission taking place in the blue luminescence (BL), with its maximum at 2.8–2.9 eV ($\lambda \approx 430$ nm), was reported for STO at room temperature.[21,23] This BL emission, potentially useful for optoelectronic applications, is well visible both in intrinsic samples at sufficiently high excitation intensities[21] and in suitably *n*-doped samples, in the latter case at much lower excitation intensities.[23,24] A similar BL was also observed for intense electron-beam excitation.[25,26] At low temperatures, the blue emission is accompanied by a spectrally narrow near-UV luminescence (UVL) located at 3.2 eV ($\lambda \approx 390$ nm), i.e., at band edge.[21,23,24] Moreover, in some cases, the BL may also be accompanied by a long green "tail" covering a spectrum similar to the GL discussed above but still visible at room temperature.[21,27] It is not clear what determines the appearance of this high-temperature GL com-

a)Electronic mail: lorenzo.marrucci@na.infn.it.

ponent, but the surface state of oxidation seems to play an important role.[21] This GL is clearly visible at high excitation intensities.[28,29]

The underlying nature of this room temperature BL is still far from clear. Although the BL yield is enhanced by *n*-doping, its spectrum looks nearly identical for different kinds of doping as well as for intrinsic samples under intense excitation (but this is only true at room temperature, as we will see below),[21,24,29] thus pointing to a role of CB electrons rather than donor levels in the enhancement.[24] When studied as a function of temperature, in contrast to the GL that vanishes quickly above 30–50 K, the BL exhibits a yield that is steadily increasing with temperature, reaching a maximum at about 160 K and then decreasing slowly (a faster decrease is, however, observed at temperatures substantially higher than room temperature, as we will see below).[21,30] Studied as a function of the excitation fluence (for short laser pulse excitation), the BL yield shows no saturation up to very high fluences, in the mJ/cm^2 range, while the low-temperature GL has a much smaller saturation threshold.[21,28] More precisely, a detailed recent study by Yasuda *et al.*[31] showed that in pure STO the BL yield is actually *quadratic* in the excitation pulse fluence up to about 1 mJ/cm^2. Above this value, there is initially a crossover to an approximately linear behavior, and then at 30–40 mJ/cm^2, there is a full saturation.[21,28,31] A strong dependence of the BL spectrum and yield on a previous surface treatment with fluorhydric acid has also been reported,[27] possibly pointing to a role of the surface or of other crystal imperfections in the luminescence process, although these results could also be explained as resulting from a variation in the surface-induced fluorescence quenching, thus unrelated to the radiative process itself (in Ref. 27 the excitation wavelength was 325 nm, at which the penetration length in STO is of only a few tens of nanometers, thus enhancing the role of the surface).

Even more intriguing is the PL dynamical behavior studied as a function of time following a very short pulse excitation. It is clearly established that the PL decay does not follow a simple exponential behavior. At low temperatures, the GL band is associated with a slow power-law decay, with a very strong temperature dependence, typical of an untrapping-rate-limited "bimolecular" dynamics.[15,16,21] We have studied the BL dynamics in detail as a function of excitation energy (in a strong excitation regime), and we have observed an interesting nonlinear dynamics, which can be modeled as a quite simple two-component decay.[28] One component seems to be exponential, or "unimolecular," while the other one can be fitted well by a bimolecular power-law decay.[28] Although apparently similar to the bimolecular behavior of GL seen at low temperatures, the BL one is much faster (also at low temperatures) and hence must be ascribed to a different process.[21] The two dynamical components are present in the whole BL spectrum, including its green tail, apparently with no significant wavelength dependence.[28] Doped samples exhibit a similar two-component dynamics as pure ones and, at high excitation fluences, also similar decay times and yields, with no evident doping-induced enhancement.[29] However, as shown by Yasuda *et al.*,[31] at smaller excitation intensities both the overall luminescence yield and the exponential decay rate of the unimolecular component are found to be strongly dependent on the dopant concentration. In the same paper, in contrast to our previous results, Yasuda *et al.* claimed that the two-component decay is actually best described by an Auger trimolecular process acting together with the unimolecular one, thus leaving the issue of the leading recombination process governing the PL decay undecided. Properly assessing the strength of the Auger recombination may be important for proposed applications of STO in optothermionic refrigeration.[32] We will come back to this issue below.

In this work, we investigate further the physics underlying the BL of STO by analyzing the PL spectra and temporal decays, for both intrinsic and doped samples, as a function of excitation energy and temperature. The temperatures of our measurements are high enough to make the activated luminescence quenching evident. Moreover, we compare in detail the predictions of different models for the PL dynamical behavior in order to establish the nature of the recombination processes involved in the decay and to shed light on the underlying electronic mechanisms.

This paper is structured as follows. Section II describes the experimental procedures. The wavelength-resolved studies as a function of excitation energy and temperature are reported and analyzed within a simple model in Sec. III. The corresponding time-resolved studies are then reported in Sec. IV, together with a first phenomenological modeling. In Sec. V we tackle the question of a more detailed modeling of the dynamical behavior. Section VI includes a discussion of the physics underlying the dynamical models used for interpreting the PL decay and a summary of our main results.

II. EXPERIMENTS

The samples used in this work were of the following three kinds: (i) five stoichiometric (100)-oriented I-STO single crystals, $1\times5\times5$ mm^3 in size, produced by four different companies (SurfaceNet GmbH, CrysTec GmbH, Crystal GmbH, and eSCeTe B.V.) by the flame-fusion Verneuil method, with specified impurity levels all below 150 ppm, and used as received; (ii) two samples of Nb-doped STO (N-STO) crystals, with a Nb molar concentration of 0.2% and having the same orientation and geometry as the I-STO samples; (iii) one sample doped with oxygen vacancies (O-STO), obtained from a pure sample by annealing for 1 h at 950 °C and 10^{-9} mbar (base pressure of 10^{-11} mbar). While I-STO samples look transparent and are verified to be good insulators, both N-STO and O-STO samples look black/dark-blue opaque and are conducting. In O-STO, from resistivity measurements performed on a thin film annealed by the same procedure, we estimate an induced carrier density of 3×10^{17} cm^{-3}, or about 0.002%, rather small but still much higher than typical residual oxygen vacancy concentrations in nominally stoichiometric samples.[29] I-STO and N-STO samples did not show aging or a hysteretic behavior due to oxygen exchange with atmosphere, as we checked by repeated measurements. Instead, O-STO samples turned transparent again when heated above 250 °C in air, clearly showing a reoxidation of the vacancies. For this reason, all our

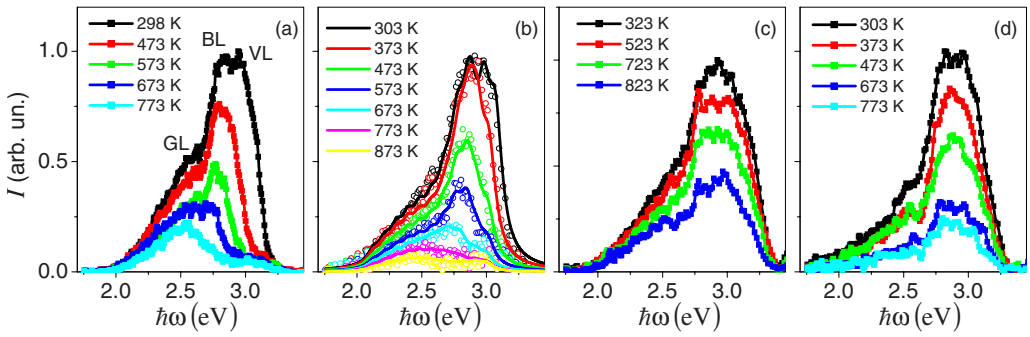

FIG. 1. (Color online) PL spectra from [(a) and (b)] I-STO and [(c) and (d)] N-STO samples at various temperatures and at an excitation fluence of [(a) and (c)] 2.2 mJ/cm^2 or [(b) and (d)] 22 mJ/cm^2. Labels GL, BL, and VL (green, blue, and violet luminescence) in (a) mark the peaks of the three separate luminescence bands that can be singled out in our spectra. A blue-to-green spectral transition (a redshift of the peak) of the PL is seen in the I-STO spectra, while it is absent in the N-STO-doped samples. The lines in (b) are best-fit curves based on our theory. The lines in the other panels are guides to the eye.

temperature behavior studies were limited to I-STO and N-STO samples. During measurement, the samples were held into a thermostat for temperature control to within 0.1 K (with an accuracy within a few kelvins). The temperature was scanned between 300 and 900 K.

In all our experiments, the excitation was induced by 3.49 eV UV photons ($\lambda = 355$ nm) in 25-ps-long laser pulses at a 10 Hz repetition rate focused to a Gaussian spot having a radius of 1.2 ± 0.1 mm at $1/e^2$ of maximum. The energy per pulse was varied from 40 μJ to 2 mJ, corresponding to an excitation fluence U ranging from a minimum of 2 to a maximum of 100 mJ/cm^2 (a value at the spot center, corresponding to twice the spatial-average value). This goes up to much higher values than those investigated by others, including Mochizuki *et al.* (up to 14 mJ/cm^2)[21] and Yasuda *et al.*[31] (up to 10 mJ/cm^2). For our highest fluence of 100 mJ/cm^2, taking into account the 25% reflection and assuming an optical penetration length of about 1 μm,[4] we estimate a peak density of photogenerated electron-hole (e-h) pairs as high as 1.2×10^{21} cm^{-3}. This corresponds to a fluence-to-density conversion factor (FDCF) $\alpha = 1.2 \times 10^{22}$ cm^{-1}/J. It must be noted, however, that the UV penetration length is highly uncertain, as different samples have shown fairly different absorption edges in previous reports. We stress that, despite our large excitation fluences, no visible photoinduced damage of the sample surfaces was induced during our experiments, and we never observed irreversible variations in the signal as a function of excitation intensity.

The luminescence emitted from the sample was collected by a lens system imaging the illuminated sample spot onto the detector head after blocking the (much stronger) elastic scattering by a long-pass filter with a cutoff wavelength of 375 nm. When recording the luminescence spectra, for detection we used a grating monochromator and a photomultiplier and integrated the signal in time (with a 50 ns time gate). In time-resolved measurements, the luminescence was instead detected with a photodiode (PD) having a rise time of about 150 ps. In time-resolved experiments, the entire luminescence spectrum was integrated. The PD signal was acquired by a 20 Gsample/s digital oscilloscope having an analog bandwidth of 5 GHz. The response function $r(t)$ of this apparatus was acquired by measuring the signal given by the elastic scattering of the excitation pulse (taken after removing the long-pass filter).

III. MEASUREMENT RESULTS: SPECTRA

The data shown in Fig. 1 refer to a typical I-STO [panels (a) and (b)] and a typical N-STO sample [panels (c) and (d)] under 2.2 mJ/cm^2 [panels (a) and (c)] and 22 mJ/cm^2 [panels (b) and (d)] excitation fluences, respectively. It is seen that the overall shape of all spectra is asymmetrical, with both GL and BL emissions present and clearly distinguishable at all temperatures in spite of a substantial overlap. At a closer inspection, an additional spectral contribution apparently located at about 3.0 eV ($\lambda \approx 400$ nm, in the violet), henceforth called violet luminescence (VL) [see panel (a)], can be singled out, particularly in I-STO samples (it is, however, possible that this emission is actually the same as the UVL band mentioned in Sec. I after a reshaping due to the detection-line long-pass filter used in our setup). This VL appears as a small shoulder in the lower temperature measurements, while it is more clearly separated, although strongly depressed, at higher temperatures. Our spectra are qualitatively consistent with literature data. Three distinct emissions with similar spectral positions were reported in Ref. 21, though at lower temperatures. The spectrum of La-doped STO reported in Ref. 24 closely resembles that of our N-STO samples at 300 K. However, compared to previous data, ours seem to show a comparatively higher yield in the GL region. In all samples, the GL contribution appears to increase more weakly than the BL one for an increasing excitation intensity, as can be seen in Fig. 1 by comparing panels (a) with (b) and (c) with (d). Therefore, the GL emission is probably more saturated than the BL one, pointing to the presence of different classes of emitters as responsible for the two bands.

As a function of temperature T, the most striking feature seen in the PL spectra is a strong redshift of the BL maximum occurring for increasing T in I-STO samples. I-STO samples at high temperatures emit almost exclusively in the green, with only a small residual emission in the blue (which we ascribe to the VL band). This blue-to-green thermal transition of the luminescence can be clearly seen even with the naked eye. The fact that this shift does not occur (or is very small) in N-STO-doped samples makes the spectra of I-STO and N-STO samples become very different at high temperatures. This is an important observation, as it is the first clear qualitative difference seen in the luminescence spectra of

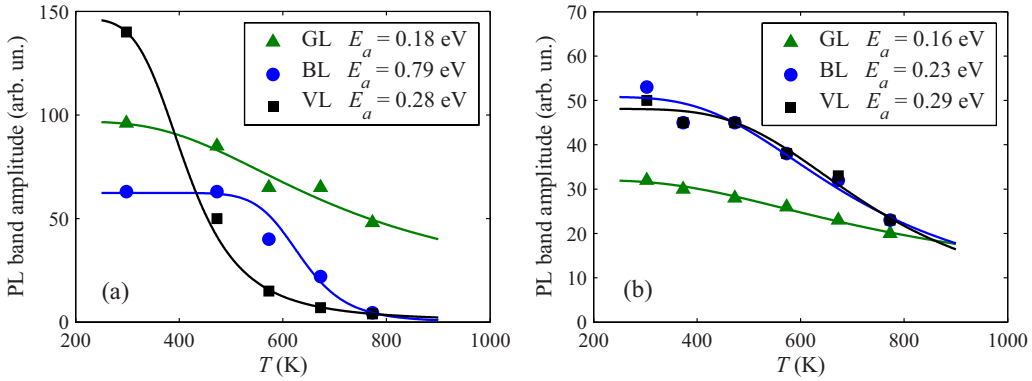

FIG. 2. (Color online) Temperature behavior of the amplitudes of the three spectral bands GL (triangles), BL (circles), and VL (squares), as seen in the (a) I-STO and (b) N-STO PL. The excitation fluence was 2.2 mJ/cm^2. Solid lines are best fits based on Eq. (2); the resulting activation energies are reported in the legend. The case of high excitation fluence (22 mJ/cm^2) gives similar results, except for a slightly smaller activation energy of the VL component (≈0.2 eV instead of ≈0.3 eV).

doped samples as compared to pure ones. In contrast to what was stated before,[24,31] this shows that the role of doping is not limited to introducing additional charge carriers in the system but somehow affects also the properties of the radiative and/or nonradiative recombination centers.

In order to analyze the data quantitatively, we will refer to a specific model for the spectral shape $I(\omega)$ of each component of the luminescence spectrum (GL, BL, and VL), treating them as independent. As previously stated, the low-temperature GL was interpreted in a quantitative way by Leonelli and Brebner[15] in terms of the annihilation of STEs of a given energy E_0. In this picture, the broadening of the band is due to the random emission of several optical phonons, each with energy $\hbar\Omega \approx 90$ meV, giving rise to the following expression:

$$I(\omega) = I_0 e^{-S_0} \sum_{n=0}^{\infty} \frac{S_0^n \Gamma/(2\pi n!)}{(E_0 - \hbar\omega - n\hbar\Omega)^2 + (\Gamma/2)^2}, \tag{1}$$

whose key parameter is the Huang–Rhys factor S_0, related to the strength of the electron-lattice interaction and fixing the average number of emitted phonons per recombination. Γ is the width of the band associated with a given n-phonon process, taken to be Lorentzian. Although devised for STEs, Eq. (1) applies equally well to the case of defect-assisted recombinations—in which defects mediate the coupling of the electronic excitation to the lattice—so it may be actually considered as a semiphenomenological model that can describe different microscopic scenarios. Leonelli and Brebner found that a value as high as S_0=5.7 produced a nice fit to the data, meaning that the maximum of intensity at 2.4 eV is well shifted with respect to the intrinsic exciton energy, taken at $E_0 \approx 2.9$ eV. We plotted the $I(\omega)$ resulting from Eq. (1), keeping the same quoted values of the parameters S_0 and E_0 and assuming a broadening factor Γ=0.12 eV: even with no adjustable parameters (except for the overall amplitude scale), we could describe in this way quite accurately the GL band shape in the region where it is well separated from the other bands [see, e.g., the highest temperature spectrum in Fig. 1(b)]. Hence, we assumed that the GL band keeps the same form in all spectra, except for a temperature-dependent scale factor, and turned to the problem of the BL and VL bands. Tentatively, given its general applicability, we used Eq. (1) also for these bands, and after suitable adjusting of the parameters E_0 and S_0, we could achieve a satisfactory fit of all data. The phonon energy $\hbar\Omega$ and the irrelevant broadening factor Γ were always kept fixed at 88 and 0.12 meV, respectively, without any attempt of optimization. The optimal values of the characteristic energies and of the Huang–Rhys factors for the GL, BL, and VL components were determined by a global fit procedure as ≃2.9, ≃2.9, and ≃3.0 eV and ≃5.5, ≃1, and ≃1, respectively, independently of fluence and temperature and allowing for only a slight sample dependence. In addition, we used as free fit parameters the respective amplitudes I_0 of the three bands at each temperature. Typical results for pure and doped samples are reported in Fig. 2. As a last step, we observed that allowing for a slight decrease in the characteristic energy of the VL contribution for increasing temperature (in any case below 0.1 eV), the fit was further improved. This shift can be probably associated with the known temperature dependence of the STO gap.[33] An example of the fit results is given in Fig. 1(b). The overall fit quality is as good in all investigated I-STO and N-STO samples.

Figure 2(a) shows that the blue-to-green transition of I-STO samples can be explained as a thermal quenching of the VL and BL components occurring at temperatures lower than that for the GL one. This is not the case for N-STO samples, for which the three amplitudes have a more similar behavior with temperature, as shown in Fig. 2(b). The thermal quenching of the PL amplitudes $I_0(T)$ can be approximately modeled by the following standard Arrhenius activation law:

$$I_0(T) \propto \tau(T) \propto [a + be^{-E_a/(k_B T)}]^{-1}, \tag{2}$$

where τ is the characteristic PL decay time, E_a is an activation energy giving the potential barrier of the competing nonradiative relaxation channels, k_B is the Boltzmann constant, and a and b are constants that give the relative weight of the temperature-independent (typically radiative) and thermally activated (typically nonradiative) contributions to the decay, respectively. The best-fit results based on Eq. (2) are also shown in Fig. 2. The corresponding activation energies are all of the order of tenths of eV, with somewhat smaller values

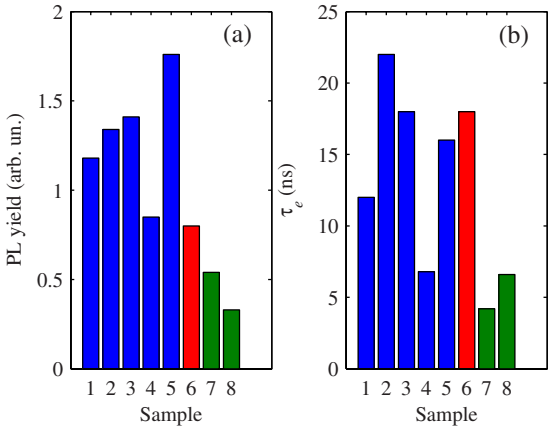

FIG. 3. (Color online) Histogram of the (a) PL yield and (b) PL-tail exponential decay time τ_e for different samples at room temperature. Samples 1–5 are I-STO (blue online), sample 6 is O-STO (red online), and samples 7–8 are N-STO (green online).

for GL (0.16–0.18 eV) and slightly larger for BL and VL (0.23–0.29 eV), with the exception of the BL in I-STO, which is found to be about 0.8 eV. According to these best-fit results, the stronger thermal quenching of the BL and VL bands compared to GL is not associated with a smaller activation energy (it is actually larger) but with a relatively larger weight of the nonradiative channels with respect to the radiative ones.

Finally, the spectrally integrated PL yield at a pump fluence of 2.2 mJ/cm^2 as a function of the sample at room temperature is shown in Fig. 3(a). The most important things to notice here are the following: (i) there is a significant sample-to-sample dependence of the yield in nominally identical I-STO samples; (ii) doped O-STO and N-STO samples do not show any enhanced yield despite the presence of many additional donor defects. We will discuss these findings in Sec. VI.

IV. MEASUREMENT RESULTS: TEMPORAL DECAYS

A typical set of PL temporal decays measured from an I-STO sample for various excitation pulse fluences U is shown in Figs. 4 and 5. The case of N-STO is very similar (an example is reported in Fig. 2 of Ref. 29). As already noted in our previous works and as confirmed by Rubano *et al.*[28,29] and Yasuda *et al.*,[31] the PL initial decay becomes faster for higher excitation energies, while the final part of the decay (the tail) varies only in its amplitude, relative to the peak, but not in its rate. One can therefore phenomenologically single out two distinct regimes: the initial fast decay, with an excitation-dependent characteristic decay time, and the final tail, with a well defined, excitation-independent exponential decay time τ_e. In I-STO, the fast decay is typically in the range of 1–2 ns (for our excitation fluences) and is only weakly sample dependent, while the slow tail time constant ranges from 6 to 23 ns, depending on the sample, as shown in Fig. 3(b). In N-STO, the fast decay rate is of the same order as in I-STO, while the exponential decay becomes somewhat faster ($\tau_e \approx 5$ ns), as an effect of doping.[31]

In Figs. 4 and 5, the decay signals are normalized to their maximum for clarity. However, also the PL signal amplitude varies strongly with the excitation intensity. More precisely, as mentioned in Sec. I, we observed an approximately linear dependence of the time-integrated PL signal, i.e., of the overall PL yield, on excitation fluence up to 30–40 mJ/cm^2, while for even higher fluences we find a saturation (see Fig. 2 of Ref. 28 and Fig. 3 of Ref. 29). The PL signal maximum typically shows a mixed linear-quadratic behavior with excitation fluence, with a relatively large scatter of the data, for reasons which we have not yet identified. The exact threshold for saturation is also sample dependent, pointing again to an important role of the defects in the PL radiative channels. Moreover, the linear yield behavior we find in our data is actually already a partly saturated one; as for lower excitation fluences, a quadratic behavior is observed instead.[31]

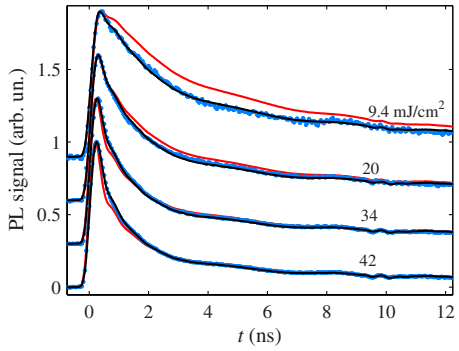

FIG. 4. (Color online) Time decay of the PL signal of an I-STO sample following its excitation by a UV picosecond pulse for different excitation fluences at room temperature. Data are shown as gray dots (blue online). The solid lines are the result of a global best fit based on our models [including a final convolution with the measured instrumental response time $r(t)$]. The black line is based on the C2PUBv1 bimolecular model, and the gray line (red online) is based on the 1PUT trimolecular model. Data and curves referring to different fluence values are vertically shifted for clarity.

To specify a characteristic experimental decay time for each given PL signal, we use its full-width-at-1/e-of-the-maximum (FW1/eM) time $t_{1/e}$. Equivalently, its inverse $t_{1/e}^{-1}$ provides a characteristic decay rate. The measured decay rates $t_{1/e}^{-1}$ versus the excitation fluence U, for different temperatures, in an I-STO sample, are

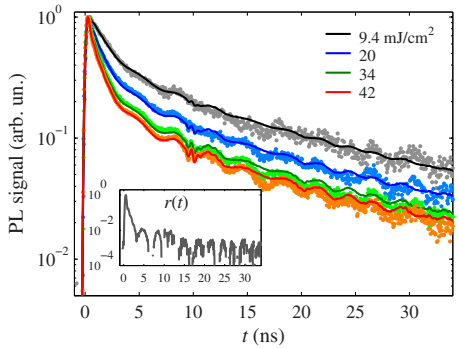

FIG. 5. (Color online) Time decays of the PL signal of an I-STO sample at room temperature for different excitation fluences, shown here in semilogarithmic scale to highlight the exponential PL tail. Data are shown as dots, while the solid lines are the result of a global best fit based on the C2PUBv1 model. The wiggles seen in the tail for both data and model predictions are due to the detection-system response function $r(t)$, which is shown in the inset (inset axis labels and units are the same as those for the main panel).

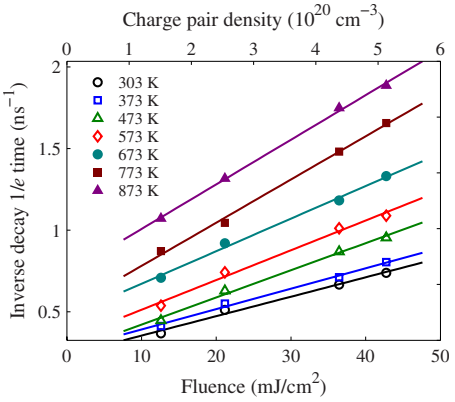

FIG. 6. (Color online) Experimental decay rates as a function of excitation fluence and temperature for the an I-STO sample. The decay rate is here defined as the inverse of the FW1/*e*M decay time $t_{1/e}$. The upper x axis gives our estimate of the density of photoinduced e-h pairs after excitation. The lines are linear best fits of the fluence dependence.

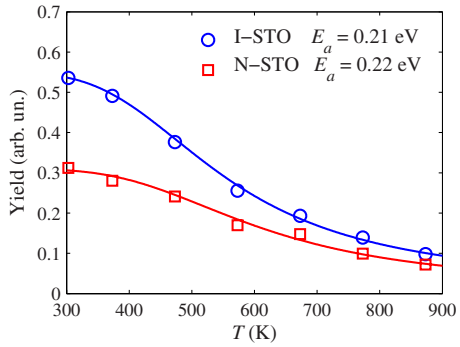

FIG. 8. (Color online) PL yield, computed from the time integral of the decay signal, as a function of temperature for I-STO and N-STO samples. Solid lines are best fits based on the activated behavior given by Eq. (2). The resulting activation energies are given in the legend.

shown in Fig. 6. N-STO samples give very similar results. In the investigated range, this decay rate shows an approximate linear dependence on the excitation fluence, as shown in the figure. However, since the measured decay times $t_{1/e}$ are close to the characteristic response time of our detection apparatus, these raw data for $t_{1/e}$ are significantly larger than the actual decay times of the luminescence. To take care of this, in principle we should deconvolve the measured decay signal and the response function of our setup. However, the numerical deconvolution of noisy data is known to be problematic, so that, following the standard procedure, we used the inverse approach. Given a theoretical model $I(t)$ for the PL decay containing the characteristic times to be determined as adjustable parameters, we first convolve it with the measured response function $r(t)$, thus obtaining a predicted signal $S(t)=(r*I)(t)$. The latter is then compared with the measured signal, thus finding the best-fit values of the adjustable parameters. In this way, the best-fit values of the characteristic decay times appearing as parameters in the model function $I(t)$ will correspond to actual PL decay times, without significant distortions due to the instrumental response function. The final time resolution that can be achieved with this approach is limited only by the signal-to-noise ratio of our data (typically 10^2-10^3). In this section, we wish to analyze the data without relying on too specific physical assumptions: ideally, we would like to adopt a model-independent description, postponing the analysis of specific models until Sec. V. Therefore, we adopt here the "phenomenological" model already used in Ref. 28 (corresponding to the 2PUB considered in Sec. V). According to this model, the PL intensity as a function of time is given by the sum of a pure unimolecular exponential decay with time constant τ_1 and a pure bimolecular decay with excitation-dependent time constant $\tau_2=1/(\gamma\alpha_2 U)$, where γ and α_2 are constants.[28] The fast FW1/*e*M time $t_{1/e}$ will be approximately proportional to the value of τ_2. For each given sample and temperature, we may assign a typical value to the time constant τ_2 by fixing a reference excitation fluence U_1 at which it must be evaluated. We choose here a value of U_1 that is in the order of our experimental range, i.e., $U_1=10$ mJ/cm^2.

The best-fit values of the exponential slower decay time $\tau_1=\tau_e$ and of the faster initial decay time τ_2 (at the reference fluence of 10 mJ/cm^2) for an I-STO and a N-STO samples are shown in Fig. 7 (the fit procedure is described in more detail in Sec. V). As in the case of the PL spectral amplitudes, all decay time temperature behaviors can be fitted fairly well by the Arrhenius law given by Eq. (2). The resulting activation energies are given in the figure legend and are in the range of 0.2–0.3 eV, of the same order as those obtained from the behavior of the PL band amplitudes.

To conclude this section, we report in Fig. 8 the measured temperature behavior of the PL yields obtained from

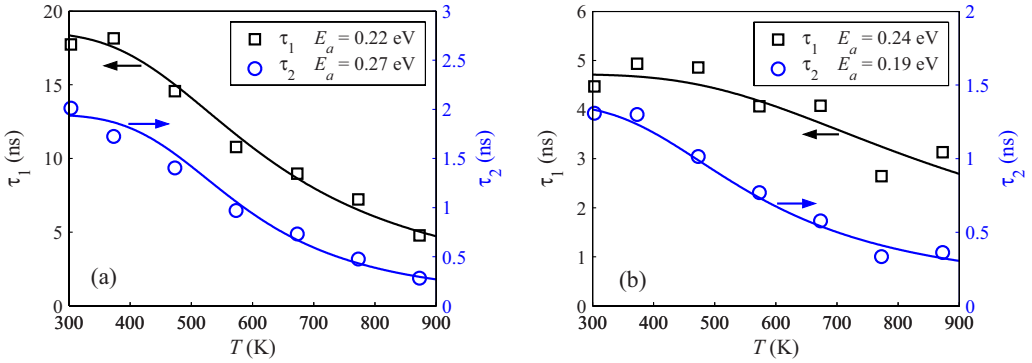

FIG. 7. (Color online) Characteristic PL decay times $\tau_1=\tau_e$ (squares) and τ_2 (circles), the latter at the reference fluence of 10 mJ/cm^2, vs temperature T for (a) an I-STO sample and (b) a N-STO sample. The lines are best fits based on the activated behavior given by Eq. (2). The resulting activation energies are given in the legend.

TABLE I. Different PL decay models tested in this work. The two best-fit values of χ^2 reported in the last two columns are averaged over different samples and repeated measurements after normalizing to the minimum χ^2 value obtained among all models for each given sample/measurement (in order to weigh all samples equally). The first χ^2 (no amplitude) is computed for decays normalized to their maximum, so that the behavior of the decay amplitude with excitation fluence does not enter the fit, and the model testing is focused on the decay rates. The second χ^2 (with amplitude) is instead computed, taking also the decay amplitudes into account. The reported differences are statistically highly significant (the formal likelihood ratio between the best model and the others is of thousands of orders of magnitude).

Model code	Rate equations	Initial conditions	Radiative term	χ^2 (no amplitude)	χ^2 (with amplitude)
1PUB	$dN/dt=-N/\tau_1-\gamma N^2$	$N(0)=\alpha U$	$I=Q\gamma N^2$	2.1	1.9
1PUT	$dN/dt=-N/\tau_1-C_A N^3$	Same as above	$I=Q\gamma N^2$	3.2	1.8
2PUB	$dN_1/dt=-N_1/\tau_1$ $dN_2/dt=-\gamma N_2^2$	$N_1(0)=\alpha_1 U$ $N_2(0)=\alpha_2 U$	$I=Q_1 N_1/\tau_1+Q_2\gamma N_2^2$	2.2	1.7
2PUT	$dN_1/dt=-N_1/\tau_1$ $dN_2/dt=-C_A N_2^3$	Same as above	$I=Q_1 N_1/\tau_1+Q_2\gamma N_2^2$	3.1	1.7
C2PUBv1	$dN_1/dt=-N_1/\tau_1-\gamma_1 N_1 N_2$ $dN_2/dt=-\gamma_2 N_2^2$	Same as above	$I=Q\lvert dN_1/dt\rvert$	1.0	1.7
C2PUBv2	Same as above	$N_1(0)=\alpha_0+\alpha_1 U$ $N_2(0)=\alpha_2 U$	$I=Q\gamma_1 N_1 N_2$	1.3	1.1

the time integral of the decays, together with the usual activation-law best fits. The resulting activation energies are again roughly consistent with the dynamical ones and with the spectral amplitude ones. No significant dependence on doping is found in this case.

V. MODELING THE TEMPORAL DECAY

Although it is firmly established that the initial decay rate of the PL at sufficiently high excitation intensities behaves nonlinearly,[28,29,31] the exact decay law and the underlying microscopic relaxation mechanisms are currently controversial, as we mentioned in Sec. I. In this section, we introduce and compare several different models for the PL decay, listed in Table I, aiming at identifying the most effective one in describing our data, which can in turn offer indications about the underlying microscopic physics (to be discussed in Sec. VI). In particular, we are especially interested in assessing the order of the leading recombination mechanism, e.g., bimolecular versus trimolecular.

Each tested model is labeled with a code (first column in Table I) that synthesizes the most important assumptions on which it is based: (i) the figure before the letter "P" gives the number of decaying electron populations considered in the model (either 1 or 2), with a "C" denoting the more specific case of coupled populations; (ii) the letters "U, B, and T" stand, respectively, for unimolecular, bimolecular, and trimolecular recombination mechanisms (a unimolecular recombination process is taken to be present in all models); "v1" and "v2" denote different variants of the same basic model.

In this work, we adopted a "global fit" procedure; that is, we fitted simultaneously all the decays measured for a given sample at a given temperature but for different values of the fluence U for a single choice of the adjustable parameters. For each model and for all samples and temperatures, we have performed global best fits of the following two kinds: (i) "without the amplitudes," i.e., on signals that had been previously normalized to their maximum; (ii) "with the amplitudes." The reason for using both methods is that the PL decay amplitudes were usually subject to a significant scatter, not present in the decay functional form, and for the highest excitation fluences also to some degree of saturation, which may not be properly taken into account in our simple models. Therefore, approach (i) is more appropriate in order to focus on the capability of our models to predict the U-dependence of the PL decay functional form and, in particular, of the PL decay rates, regardless of the amplitude behavior. Approach (ii) tests the models in their predictive power for both PL rates and amplitudes but tends to weigh more the amplitude behavior, as it gives the strongest data variations. All compared models have four adjustable parameters in approach (ii), while in approach (i) all models have three parameters except for one (C2PUBv1), which has four. For each approach, we quantified the performance of each model with the fit χ^2 (normalized to the data variance, estimated using the measured noise before the excitation pulse), averaged over different samples and repeated measurements as specified in Table I.

The first two models in Table I (1PUB and 1PUT) are based on the assumption that a single-population density $N(t)$ of decaying electrons and holes (balanced in number) suffices for capturing the recombination dynamics revealed by the PL decay. Many past analyses of picosecond-laser-induced PL temporal decays in semiconductors (see, e.g., Refs. 34–36), as well as the recent work of Yasuda *et al.*[31] on the STO, interpret the PL decay by a similar single-population model. While the unimolecular and bimolecular terms are fairly common in solid state luminescence, the appearance of a third-order trimolecular term, typically ascribed to Auger processes involving two electrons and a hole or two holes and an electron, is only seen at very high excitation densities in indirect bandgap materials. In principle, it is quite reasonable to expect this behavior in the case of STO, and indeed the 1PUT model is that assumed in Ref. 31. However, we find that the 1PUT model is very ineffective in describing our data. An example of the unsatisfactory results of a global fit based on the 1PUT model is shown in Fig. 4

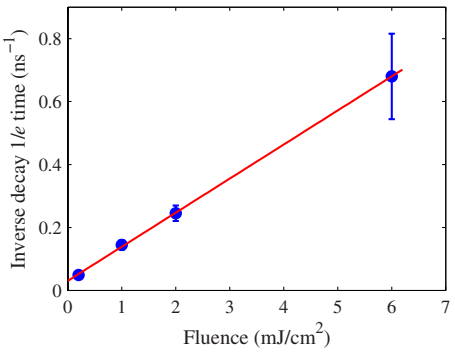

FIG. 9. (Color online) Inverse decay times vs excitation fluence for the four PL decay curves reported in Fig. 1 of Ref. 31. The times have been estimated graphically from the initial decay slope in the semilogarithmic chart. The line (red online) is a linear best fit. The good linearity of the decay rates vs fluence confirms a bimolecular behavior for the initial fast decay.

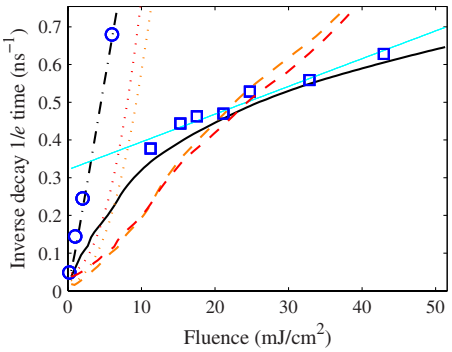

FIG. 10. (Color online) Inverse decay rates vs fluence as measured for an I-STO sample (squares) and as predicted by different models (lines) after a global best fit on the measured decays. Besides ours, the data of Yasuda *et al.* (already given in Fig. 9) are also plotted (circles). The two sets of data do not merge into a single smooth behavior because of the much slower response of our apparatus as compared to that used by Yasuda *et al.* in Ref. 31. The predictions of the C2PUBv1 model (black lines), after a global fit on our data only, explain both our data (solid line, obtained after a convolution with our instrumental response function) and the data of Yasuda *et al.* (dot-dash line, obtained from the C2PUBv1 model assuming an instantaneous instrumental response). Dashed and dotted curves correspond to the predictions of the 1PUT model (gray line, red online) and of the 2PUT model (light gray line, orange online) after convolution with our response function (dashed lines) or for an instantaneous response (dotted lines). The gray solid line (cyano online) is a linear best fit to our data.

(gray lines, red online), while the average best-fit χ^2 values relative to the best-performing models are reported in Table I.

We stress that by using a global (simultaneous) fit on all the decays obtained at different excitation energies U, we have put the models to the test not only on their capability to predict the single-decay functional form, but also on their capability to predict the overall dependence of this functional form on the excitation fluence U. This dependence is very sensitive to the order of the highest nonlinear term in the decay equations, and therefore matching this dependence provides a much stricter test than matching the single-decay behavior. More precisely, the initial rate of decay taking place shortly after excitation is predicted to depend much more strongly on the excitation fluence U for the 1PUT model than for a second-order model, such as 1PUB (see Table I). Indeed, assuming that the PL signal is generated by a given power p of the population density, $I(t) \propto N^p(t)$ (e.g., $p=2$ for a bimolecular radiative recombination), the initial logarithmic decay rate for a single-population model including both bimolecular and trimolecular terms is given by

$$-\left.\frac{d\ln I}{dt}\right|_{t=0^+} = -\left.\frac{p}{N}\frac{dN}{dt}\right|_{t=0^+} = p\left[\frac{1}{\tau_1} + \gamma N(0^+) + C_A N^2(0^+)\right] = p\left(\frac{1}{\tau_1} + \gamma\alpha U + C_A\alpha^2 U^2\right). \tag{3}$$

Thus, for the 1PUT model, one would expect a quadratic dependence of this initial decay rate on excitation fluence U, while for a second-order (bimolecular) model, having $C_A \approx 0$, one expects a linear dependence. This initial decay rate is well estimated by the inverse FW1/eM time $t_{1/e}^{-1}$. We indeed find a linear behavior, as shown in Fig. 6, and this supports a bimolecular model. To investigate also the hypothesis of a crossover from a trimolecular behavior taking place for the lower fluence range studied by Yasuda *et al.* (0–10 mJ/cm^2) to a bimolecular one in our higher range of fluences (10–50 mJ/cm^2), we graphically extracted from Fig. 1 of Ref. 31 the initial logarithmic slope of the four reported decays. These values are plotted in Fig. 9 versus the excitation fluence, showing that the behavior is again perfectly linear in U, as expected from a bimolecular model (not necessarily a single-population model), and hence not consistent with a third-order model such as 1PUT. We note that the fluence dependence of the measured decay rates can be altered by the finite response function of the apparatus. The data from Ref. 31 were taken with a streak camera, which typically has a very fast response in the picosecond range, so that they should not be affected by this problem. Our data are instead affected by the slower response time of our equipment. Nonetheless, even after convolution with the response function, the 1PUT third-order model predicts a stronger dependence of the initial decay rate on the excitation fluence than what is seen in our data, as shown already in Fig. 4 and more explicitly in Fig. 10.

In synthesis, we can conclude that the initial faster decay is a second-order, or bimolecular, recombination process, and no significant trimolecular effect is detected in our data. We note, however, that even at fluences much smaller than ours, indirect semiconductors usually exhibit a strong Auger-like third-order decay.[34–36] Presumably, third-order Auger interactions are depressed in STO by its relatively large bandgap[37] and high dielectric constant, while bimolecular recombinations might be favored by its comparatively large density of intragap trapping states and by its stronger electron-phonon interactions.

Although it behaves much better than the trimolecular model, we see from Table I that also the bimolecular single-population model 1PUB is not fully satisfactory in describing our data. For this reason, we decided to consider models based on two dynamical populations, $N_1(t)$ and $N_2(t)$, representing, for example, free and trapped charges. The simplest model of this kind is the one already considered in our previous papers,[28] labeled as 2PUB, which corresponds to the case of two independent populations, one decaying with a

unimolecular process and the other with a bimolecular one (see Table I). The best fits obtained using this model are fairly good, but again not fully satisfactory. Moreover, this model does not lend itself to a simple and plausible physical interpretation. However, this 2PUB model has the advantage of having two well separated terms describing the initial faster decay and the final slower tail. Therefore, it is particularly apt to phenomenologically describe the data, for characterizing the faster and slower decay rates of our data in a roughly model-independent way, as we have done in Sec. IV. For the sake of completeness, we also considered a two-population unimolecular and trimolecular model (2PUT), which, however, can be discarded after a comparison with the data (see, e.g., Fig. 10).

To go beyond the 2PUB model while remaining in the framework of a two-population model, it is therefore necessary to assume some kind of coupling between the two populations (C2PUB models). The simplest choice is to include a term proportional to the cross product N_1N_2 in one of the rate equations, i.e., a recombination process of one population that is stimulated (or assisted) by the other population. This may arise from a variety of processes, as will be discussed in the Sec. VI. The solution to C2PUB rate equations (with the more general initial conditions given in the table for C2PUBv2, see below) is the following:

$$N_1(t) = \frac{(\alpha_0 + \alpha_1 U)e^{-t/\tau_1}}{(1 + t/\tau_2)^{\gamma_1/\gamma_2}},$$

$$N_2(t) = \frac{\alpha_2 U}{1 + t/\tau_2}, \tag{4}$$

with $\tau_2 = 1/(\gamma_2 \alpha_2 U)$. The model must be now completed with an assumption about the radiative terms. We consider here two different possible choices for this assumption, leading to the two model variants given in Table I. The first (C2PUBv1) is obtained from the assumption that both recombination terms in the N_1 population are partly radiative, with the same quantum efficiency Q. With this assumption, the predicted PL decay is given by the following expression (in which we have also set $\alpha_0 = 0$, as otherwise we would get an absurd nonzero PL for zero excitation):

$$I(t) = Q\left|\frac{dN_1}{dt}\right| = k_1 U \frac{e^{-t/\tau_1}}{(1 + t/\tau_2)^{\gamma_1/\gamma_2}} + k_2 U^2 \frac{e^{-t/\tau_1}}{(1 + t/\tau_2)^{1+\gamma_1/\gamma_2}}, \tag{5}$$

where k_1 and k_2 are constant amplitudes, and the following relationship holds between the parameters:

$$\frac{\gamma_1}{\gamma_2} = \frac{k_2 \tau_2 U}{k_1 \tau_1} = \frac{k_2}{k_1 \tau_1 \gamma_1 \alpha_2}. \tag{6}$$

From our best fits, we obtain a typical ratio $\gamma_1/\gamma_2 = 0.1-0.3$.

This model is in very good agreement with our data (for normalized decays), as shown, for example, in Figs. 4 and 10. Figure 10 also shows that the C2PUBv1 model, after fixing its parameters to those giving a best fit to our data, also predicts well, without any further adjustment, the decay rates measured by Yasuda *et al.*[31] for a smaller excitation fluence range. The advantage of the C2PUBv1 model, compared to the previously mentioned ones, is also quantitatively reflected in the normalized χ^2 of the fit, which is smaller than that for the other models by a factor of 2 or 3, statistically very significant. However, when comparing normalized decays, this model has one adjustable parameter more than the others (four against three), so that there is still room for doubt. Moreover, when fitting also the PL amplitudes, this model does not perform much better than the others. This is probably revealing some saturation behavior of the amplitude data that is not well captured by this model.

Let us now consider the second variant of the C2PUB model (C2PUBv2) that is obtained by the following assumption: the radiative emission is now taken to arise only from the coupling term N_1N_2, i.e., from the decays involving both populations 1 and 2. Mathematically, this is equivalent to setting $k_1 = 0$ in Eq. (5). The number of adjustable parameters is thus back to 3 in the case of normalized decays. Nevertheless, this C2PUBv2 model is almost as effective as C2PUBv1 in the global best fits on normalized decays. In the best fits including also the decay amplitudes (i.e., in approach ii), as can be seen from the χ^2 values given in Table I, this model is actually giving by far the best results (using the same number of adjustable parameters as for other models) provided that we use the modified initial conditions indicated in Table I with $\alpha_0 \neq 0$. This corresponds to a saturated dependence of $N_1(0)$ versus U and mathematically leads to the replacement $k_2 U \rightarrow (k_{21}U + k_{22}U^2)$ in Eq. (5) [since we know that $\gamma_1 \ll \gamma_2$, we also set $\gamma_1 \approx 0$ in Eq. (5) in order to keep the number of adjustable parameters to 4]. This modification of the initial conditions does not affect the best fits on normalized decays because it alters only the predicted PL amplitudes but not the decay rates and functional forms. As we will discuss in the Sec. VI, this modified choice of initial conditions also lends itself to a simple and plausible physical interpretation.

Before concluding this section, we note that for $\tau_1 \gg \tau_2$, both models C2PUB (v1 and v2) predict an initial time decay of the PL of the form $I(t) \sim 1/(1 + t/\tau_2)^{(1+\gamma_1/\gamma_2)}$, which, for small values of the ratio γ_1/γ_2 such as those found in our best fits, is very similar to that predicted by trimolecular models, i.e., $I(t) \sim 1/(1 + t/\tau_2)$. The other bimolecular models, 1PUB and 2PUB, that we analyzed predict instead an initial behavior that is inversely quadratic rather than linear in time, i.e., $I(t) \sim 1/(1 + t/\tau_2)^2$. This fact probably explains why Yasuda *et al.*, when fitting the single-decay curve, found a better fit for their decays using a trimolecular model rather than a single-population bimolecular one. On the other hand, our global fits discriminate much more effectively among the various possible models.

VI. DISCUSSION AND CONCLUSIONS

We now turn to discussing the microscopic physics that may underly the STO blue PL phenomena we have described. The photogenerated carriers may, in principle, populate different excited states, which can be both localized (trapped) or extended (mobile). Mobile charges will belong

to the STO CB as electrons and to the VB as holes, in both cases probably with some degree of phonon dressing (large polarons). Localized charges may, in principle, be self-trapped and fully intrinsic (small polarons, or STEs if paired) or associated with intrinsic crystalline disorder or defects such as oxygen vacancies, dislocations, or possibly surface states. The indirect nature of the STO bandgap forbids CB-VB direct recombinations, so that electron coupling to phonons, presumably enhanced by defect trapping or self-trapping, is an essential element of the luminescence process.

Let us start by discussing the spectral and yield features of the PL in order to identify the nature of its radiative centers and of the competing nonradiative channels that may contribute to its quenching at high temperature. According to our fits of the PL spectra, the typical total energy released by the annihilation of an e-h pair is $\simeq 2.9$ eV, partly dissipated in phonons and partly radiated. The redshift of the GL spectral component with respect to the BL and VL components is attributed to the larger fraction of vibrational energy released in the former case, implying a stronger electron-phonon coupling. The radiative processes giving rise to the PL can be, in principle, fully intrinsic, i.e., characteristic of a perfect STO crystal, such as phonon-assisted CB-VB direct recombinations or STE annihilation, or again associated with intrinsic structural lattice defects such as those mentioned above.[38] Extrinsic defects such as chemical impurities are likely to be excluded, instead, because the PL yield does not present the very large sample-to-sample fluctuations that are typical of impurity-associated luminescence (see Fig. 3).[12] Moreover, the lack of any significant doping-induced enhancement of the PL yield and of its decay rate as seen in our intense excitation regime (see Fig. 3), in which the doped charge density is negligible with respect to the photoinduced one, indicates that the radiative centers are probably not to be associated with bulk oxygen vacancies, Nb ions, or other donor centers, in contrast to what is often stated in the literature.[39] This is to be contrasted with the regime of low excitation intensity, in which doping-induced electrons are not negligible and doped samples do show a greatly enhanced yield and decay rate of the PL.[21,23,24,31] The small, but significant, sample-to-sample fluctuations of PL yield and decay rate that we see and the presence of three different spectral components in the PL spectra having different thermal behaviors concur to indicate that a significant role in the STO luminescence is played by unidentified intrinsic defects (other than standard bulk oxygen vacancies), most likely by providing the radiative centers responsible for the luminescence itself. A less likely alternative hypothesis is that the luminescence is a fully intrinsic process (e.g., taking place in STEs) and the defect role is that of introducing competing nonradiative decay channels that decrease the yield. In both cases, the responsible defects might be titanium interstitials,[26] crystal dislocations,[40] or other defect complexes[26,41] or, possibly, surface defects, as suggested by the strong PL enhancement seen in acid-etched samples and in STO nanoparticles.[27,42] On the possible role of the surface states, see also Ref. 43. However, the PL spectral difference between the Nb-doped and pure samples that we observed at high temperatures remains unexplained.

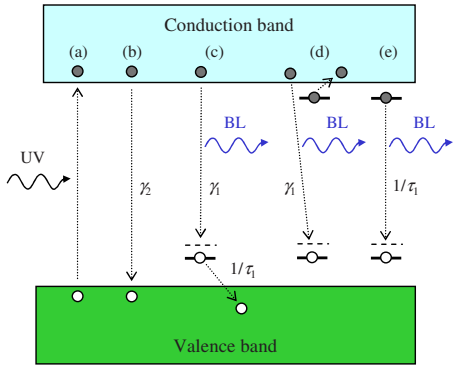

FIG. 11. (Color online) Schematic picture of the main electronic processes that may be postulated for interpreting the rate equations of our decay models C2PUB v1 and v2: (a) pump photon (UV) absorption and e-h pair generation, (b) nonradiative direct e-h recombination, and (c) radiative cross recombination between a free electron and a trapped hole, with blue photon (BL) emission and nonradiative thermal untrapping of holes, (d) radiative crossed recombination between a free electron and a trapped exciton, and (e) radiative spontaneous annihilation of a trapped exciton. The constants γ_1, γ_2, and $1/\tau_1$ are the dynamical rates of each process.

Let us now move on to discussing the physical interpretation of the PL decay dynamics that naturally emerges from our best model, i.e., C2PUB (v1 or v2), with the help of Fig. 11, which provides a schematic picture of the most important dynamical processes assumed to occur in the system. At time zero, the UV excitation will generate many e-h pairs in the CB and VB (process a), part of which will redistribute very quickly (within a time scale of a few picoseconds, negligible for our experimental resolution) in trapped states lying in the bandgap (horizontal solid lines in Fig. 11). The initial conditions given in Table I are defined by this rapid redistribution process. Most likely, the number and energy depth of these traps are not symmetrical between holes and electrons. Here, for definiteness, we assume that there are mainly trapped holes and free electrons, although the converse is equally possible. Trapped holes, or possibly trapped hole-electron pairs (i.e., trapped excitons), will form population 1 of model C2PUB, while free electrons will correspond to population 2. It is also assumed that $N_1 \ll N_2$; i.e., the trapped holes are only a small fraction of the total number, so that the free electrons and holes are approximately still balanced. These free pairs will then recombine directly in (defect-assisted or phonon-assisted) nonradiative bimolecular processes [process (b) in Fig. 11] controlled by the rate constant γ_2. This provides the faster decay channel, entirely nonradiative and (approximately) independent of the N_1 decay. The best-fit values of the time constant τ_2, combined with our estimate of the FDCF constant, leads to an estimated band-band recombination rate constant $\gamma_2 \simeq 10^{-11}$ s^{-1} cm^3. This value is intermediate between the typical orders of magnitude found for indirect and for direct semiconductors,[28] which seems a plausible result.

Thus far, the two variants of model C2PUB are essentially identical. They are, however, distinguished by the interpretation attributed to population 1 and its two decay terms. The simplest (and hence more plausible) interpretation is that corresponding to variant C2PUBv2, described by the two processes under label (c) in Fig. 11. In this case, the

unimolecular term (with a rate constant of $1/\tau_1$) is simply taken to be a (nonradiative) thermal untrapping of holes (not balanced by the trapping of free holes, except for very short times after excitation, because free holes decay much faster), while the coupling term proportional to N_1N_2 is taken to be a cross recombination between a trapped hole and a free electron, leading to the PL emission, with a rate constant of γ_1. Phonons will also be created in the emission (triggered by defect vibrational excitations, shown as dashed lines in Fig. 11), thus explaining the PL Stokes shift and the spectral shape discussed in Sec. III. The different spectral components (BL, GL, and VL) are here ascribed to the existence of different kinds of trapping sites. We also note that in the intense excitation regime in which we have performed our measurements, it is likely that the initial number of trapped holes is saturated. This would explain quite naturally the initial conditions adopted in C2PUBv2. On the other hand, for lower excitation energies, a nonsaturated linear behavior $N_1(0) \sim U$ should be resumed, thus explaining also the quadratic-to-linear yield crossover reported by Yasuda *et al.*[31]

To interpret model C2PUBv1, we must assume instead that population 1 corresponds to excitons (i.e., e-h pairs), rather than unpaired holes, that are either self-trapped or trapped near a structural defect. In this case, population 1 can decay either by spontaneous annihilation [process (e) in Fig. 11] or by "crossed" recombination of a hole of the trapped pair with a mobile electron, leading to the emission of one PL photon and the simultaneous freeing of the electron of the pair [process (d) in Fig. 11]. Both the unimolecular and the coupling terms would then be radiative with a similar quantum yield, as assumed in model C2PUBv1. Although possible in principle, we believe that this C2PUBv1 model scenario is somewhat less plausible than the former (the C2PUBv2 one), both because it is more complex and because it is difficult to justify the very rapid creation of a population of trapped excitons as would be required by the initial conditions assumed in the model.

In conclusion, the main results of the investigation reported in this article are the following: (i) we have presented strong evidence that the radiative centers involved in the BL cannot be associated with bulk oxygen vacancies or other donor impurities; (ii) we have shown, nevertheless, that a crucial role in the luminescence is played by other yet-unidentified intrinsic structural defects, such as dislocations, defect complexes, and possibly the surface; these defects likely provide the actual radiative centers; (iii) we have shown that the initial decay in the investigated excitation-intensity range is dominated by a bimolecular process, while trimolecular processes, such as the Auger process, are not significant; (iv) we have provided strong evidence that at least two separate interacting photoexcited charge populations are involved in the PL dynamics, which we interpret simply as mobile and defect-trapped charges.

[1] A. Savoia, D. Paparo, P. Perna, Z. Ristic, M. Salluzzo, F. Miletto Granozio, U. Scotti di Uccio, C. Richter, S. Thiel, J. Mannhart, and L. Marrucci, Phys. Rev. B **80**, 075110 (2009).
[2] M. Huijben, A. Brinkman, G. Koster, G. Rijnders, H. Hilgenkamp, and D. H. A. Blank, Adv. Mater. **21**, 1665 (2009).
[3] K. van Benthem, C. Elsässer, and R. H. French, J. Appl. Phys. **90**, 6156 (2001).
[4] M. Capizzi and A. Frova, Phys. Rev. Lett. **25**, 1298 (1970).
[5] H. P. R. Frederikse and W. R. Hosler, Phys. Rev. **161**, 822 (1967).
[6] D. Kéroack, Y. Lépine, and J. L. Brebner, J. Phys. C **17**, 833 (1984).
[7] D. M. Eagles, M. Georgiev, and P. C. Petrova, Phys. Rev. B **54**, 22 (1996).
[8] J. L. M. van Mechelen, D. van der Marel, C. Grimaldi, A. B. Kuzmenko, N. P. Armitage, N. Reyren, H. Hagemann, and I. I. Mazin, Phys. Rev. Lett. **100**, 226403 (2008).
[9] Y. Ishida, R. Eguchi, M. Matsunami, K. Horiba, M. Taguchi, A. Chainani, Y. Senba, H. Ohashi, H. Ohta, and S. Shin, Phys. Rev. Lett. **100**, 056401 (2008).
[10] C. Itoh, M. Sasabe, H. Kida, and K.-i. Kan'no, J. Lumin. **112**, 263 (2005).
[11] A. Stashans, Mater. Chem. Phys. **68**, 124 (2001).
[12] L. Grabner, Phys. Rev. **177**, 1315 (1969).
[13] T. Feng, Phys. Rev. B **25**, 627 (1982).
[14] M. Aguilar and F. Agullo-Lopez, J. Appl. Phys. **53**, 9009 (1982).
[15] R. Leonelli and J. L. Brebner, Phys. Rev. B **33**, 8649 (1986).
[16] T. Hasegawa, M. Shirai, and K. Tanaka, J. Lumin. **87–89**, 1217 (2000).
[17] M. Deguchi, N. Nakajima, K. Kawakami, N. Ishimatsu, H. Maruyama, C. Moriyoshi, Y. Kuroiwa, S. Nozawa, K. Ishiji, and T. Iwazumi, Phys. Rev. B **78**, 073103 (2008).
[18] Y. Qiu, Y.-J. Jiang, G.-P. Tong, and J.-F. Zhang, Phys. Lett. A **372**, 2920 (2008).
[19] L. M. Prócel, F. Tipán, and A. Stashans, Int. J. Quantum Chem. **91**, 586 (2003).
[20] R. I. Eglitis, E. A. Kotomin, G. Borstel, S. E. Kapphan, and V. S. Vikhnin, Comput. Mater. Sci. **27**, 81 (2003).
[21] S. Mochizuki, F. Fujishiro, and S. Minami, J. Phys.: Condens. Matter **17**, 923 (2005).
[22] S. Mochizuki, F. Fujishiro, K. Ishiwata, and K. Shibata, Physica B **376–377**, 816 (2006).
[23] D. Kan, T. Terashima, R. Kanda, A. Masuno, K. Tanaka, S. Chu, H. Kan, A. Ishizumi, Y. Kanemitsu, Y. Shimakawa, and M. Takano, Nature Mater. **4**, 816 (2005).
[24] D. Kan, R. Kanda, Y. Kanemitsu, Y. Shimakawa, M. Takano, T. Terashima, and A. Ishizumi, Appl. Phys. Lett. **88**, 191916 (2006).
[25] L. Grigorjeva, D. Millers, V. Trepakov, and S. Kapphan, Ferroelectrics **304**, 117 (2004).
[26] J. Zhang, S. Walsh, C. Brookds, D. G. Schlom, and L. J. Brillson, J. Vac. Sci. Technol. B **26**, 1466 (2008).
[27] Z.-h. Li, H.-t. Sun, Z.-q. Xie, Y.-y. Zhao, and M. Lu, Nanotechnology **18**, 165703 (2007).
[28] A. Rubano, D. Paparo, F. Miletto, U. Scotti di Uccio, and L. Marrucci, Phys. Rev. B **76**, 125115 (2007).
[29] A. Rubano, D. Paparo, M. Radović, A. Sambri, F. Miletto Granozio, U. Scotti Di Uccio, and L. Marrucci, Appl. Phys. Lett. **92**, 021102 (2008).
[30] Y. Yamada, H. Yasuda, T. Tayagaki, and Y. Kanemitsu, Phys. Rev. Lett. **102**, 247401 (2009).
[31] H. Yasuda and Y. Kanemitsu, Phys. Rev. B **77**, 193202 (2008).
[32] L.-l. Zhang, P. Han, K.-j. Jin, L. Liao, C.-l. Hu, and H.-b. Lu, J. Phys. D: Appl. Phys. **42**, 125109 (2009).
[33] K. W. Blazey, Phys. Rev. Lett. **27**, 146 (1971).
[34] H. J. Zarrabi, W. B. Wang, and R. R. Alfano, Appl. Phys. Lett. **46**, 513 (1985).
[35] P. T. Landsberg, Appl. Phys. Lett. **50**, 745 (1987).
[36] J. Linnros, J. Appl. Phys. **84**, 275 (1998).
[37] N. F. Massé, A. R. Adams, and S. J. Sweeney, Appl. Phys. Lett. **90**, 161113 (2007).
[38] G. F. J. Garlick, Rep. Prog. Phys. **30**, 491 (1967).
[39] H. Y. Hwang, Nature Mater. **4**, 803 (2005).
[40] K. Szot, W. Speier, G. Bihlmayer, and R. Waser, Nature Mater. **5**, 312 (2006).
[41] V. M. Longo, A. T. de Figueiredo, S. de Lázaro, M. F. Gurgel, M. G. S. Costa, C. O. Paiva-Santos, J. A. Varela, E. Longo, V. R. Mastelaro, F. S. DE Vicente, A. C. Hernandes, and R. W. A. Franco, J. Appl. Phys. **104**, 023515 (2008).
[42] W. F. Zhang, Z. Yin, and M. S. Zhang, Appl. Phys. A: Mater. Sci. Process. **70**, 93 (2000).
[43] M. Kareev, S. Prosandeev, J. Liu, C. Gan, A. Kareev, J. W. Freeland, M. Xiao, and J. Chakhalian, Appl. Phys. Lett. **93**, 061909 (2008).